



CHORUS

This is the accepted manuscript made available via CHORUS. The article has been published as:

β -delayed-neutron studies of $^{135,136}\text{Sb}$ and ^{140}I performed with trapped ions

B. S. Wang, S. A. Caldwell, N. D. Scielzo, A. Czeszumka, J. A. Clark, G. Savard, A. Aprahamian, M. T. Burkey, C. J. Chiara, J. Harker, A. F. Levand, S. T. Marley, G. E. Morgan, J. M. Munson, E. B. Norman, A. Nystrom, R. Orford, S. W. Padgett, A. Pérez Galván, K. S. Sharma, K. Siegl, and S. Y. Strauss

Phys. Rev. C **101**, 025806 — Published 24 February 2020

DOI: [10.1103/PhysRevC.101.025806](https://doi.org/10.1103/PhysRevC.101.025806)

Beta-delayed-neutron studies of $^{135,136}\text{Sb}$ and ^{140}I performed with trapped ions

B. S. Wang,^{1,2,*} S. A. Caldwell,^{3,4,†} N. D. Scielzo,¹ A. Czeszumka,^{1,2,‡} J. A. Clark,⁴
G. Savard,^{4,3} A. Aprahamian,⁵ M. T. Burkey,^{1,4} C. J. Chiara,^{4,6,§} J. Harker,^{4,6} A. F. Levand,⁴
S. T. Marley,^{7,5} G. E. Morgan,^{8,4} J. M. Munson,² E. B. Norman,² A. Nystrom,^{5,4} R. Orford,^{9,4}
S. W. Padgett,¹ A. Pérez Galván,^{4,¶} K. S. Sharma,⁸ K. Siegl,⁵ and S. Y. Strauss⁵

¹*Lawrence Livermore National Laboratory, Livermore, California 94550, USA*

²*Department of Nuclear Engineering, University of California, Berkeley, California 94720, USA*

³*Department of Physics, University of Chicago, Chicago, Illinois 60637, USA*

⁴*Physics Division, Argonne National Laboratory, Lemont, Illinois 60439, USA*

⁵*Department of Physics, University of Notre Dame, Notre Dame, Indiana 46556, USA*

⁶*Department of Chemistry and Biochemistry, University of Maryland, College Park, Maryland 20742, USA*

⁷*Department of Physics, Louisiana State University, Baton Rouge, Louisiana 70803, USA*

⁸*Department of Physics and Astronomy, University of Manitoba, Winnipeg, Manitoba R3T 2N2, Canada*

⁹*Department of Physics, McGill University, Montréal, Québec H3A 2T8, Canada*

(Dated: December 13, 2019)

Beta-delayed-neutron (βn) spectroscopy was performed using the Beta-decay Paul Trap and an array of radiation detectors. The βn branching ratios and energy spectra for $^{135,136}\text{Sb}$ and ^{140}I were obtained by measuring the time of flight of recoil ions emerging from the trapped ion cloud. These nuclei are located at the edge of an isotopic region identified as having βn branching ratios that impact the r -process abundance pattern around the $A \approx 130$ peak. For $^{135,136}\text{Sb}$ and ^{140}I , βn branching ratios of 14.6(13)%, 17.6(29)%, and 7.6(28)% were determined, respectively. The βn energy spectra obtained for ^{135}Sb and ^{140}I are compared with results from direct neutron measurements, and the βn energy spectrum for ^{136}Sb has been measured for the first time.

I. INTRODUCTION

Beta-delayed-neutron (βn) emission is a process that can occur for neutron-rich nuclei sufficiently far from stability. In this process, a precursor nucleus undergoes β^- decay to a highly excited state in the daughter nucleus above the neutron-separation energy that emits a neutron. The properties of βn -emitting nuclei are important in various areas of basic and applied sciences, including nuclear astrophysics, nuclear energy, and nuclear structure.

The astrophysical rapid neutron-capture process (r process) is believed to be responsible for the production of roughly half of the elements heavier than iron [1, 2]. In the r process, neutron-rich nuclei far from stability are produced through repeated neutron-capture reactions, and βn emission during the eventual decay back to stability impacts the final isotopic abundance pattern. Different astrophysical environments, such as core-collapse supernovae [3, 4] and neutron-star mergers [5, 6], have been investigated as possible r -process sites by comparing theoretical models with observation. These models require high-quality nuclear data, such as

nuclear masses, β -decay and neutron-capture rates, and βn -emission probabilities, for the thousands of isotopes along the nucleosynthesis pathway and populated during the decay back to stability. Much of this information still remains unknown, given the experimental challenges of accessing nuclei far from stability.

Beta-delayed-neutron emission also plays a key role in the control and safety of nuclear reactors. Both the branching ratios and energy spectra are required for reactor kinetics calculations and safety studies [7, 8]. Higher-quality nuclear data would allow for the βn yield and energy spectrum to be calculated for individual contributing isotopes, making it possible to accurately model any fuel-cycle concept, actinide mix, or irradiation history.

In addition, the information obtained in βn measurements helps to provide a better understanding of the nuclear structure of neutron-rich nuclei [9–12]. For example, measuring the βn -emission probability can be used to deduce the β -strength function above the neutron-separation energy of the daughter nucleus [13, 14]. Beta-delayed-neutron studies also help to constrain nuclear-structure calculations [15] and empirical models [16] that predict the decay properties of nuclei for which no data exist.

In this work, the Beta-decay Paul Trap (BPT) [17–19], a linear radiofrequency quadrupole ion trap with an open geometry, was utilized to study the βn branching ratios and energy spectra of a number of βn -emitting nuclei, which were produced with the Californium Rare Isotope Breeder Upgrade (CARIBU) facility [20] at Argonne National Laboratory. The results for $^{137,138}\text{I}$ and $^{144,145}\text{Cs}$ are discussed in Ref. [21], and the results for the more neutron-rich isotopes, $^{135,136}\text{Sb}$ and ^{140}I , are

* alan2@llnl.gov

† Present address: Rigetti Computing, Berkeley, California 94710, USA

‡ Present address: mittemitte GmbH, 12047 Berlin, Germany

§ Present address: U.S. Army Research Laboratory, Adelphi, Maryland 20783, USA

¶ Present address: Vertex Pharmaceuticals, San Diego, California 92121, USA

71 discussed here. Recent sensitivity studies performed by
 72 Mumpower *et al.* [22] indicate that the latter three nuclei
 73 are situated at the edge of a region in the nuclear chart
 74 where the βn branching ratios significantly impact the
 75 final r -process abundance pattern around the $A \approx 130$
 76 peak.

77 II. EXPERIMENTAL METHODS

78 In the present work, the challenges associated with
 79 direct neutron detection are circumvented by instead
 80 studying the nuclear recoil from β decay. Radioactive
 81 ions are suspended in vacuum as a $\sim 1\text{-mm}^3$ cloud at
 82 the center of the BPT. When a trapped ion undergoes
 83 β decay, the recoil ion and emitted radiation emerge
 84 from the cloud with negligible scattering, allowing for
 85 their properties to be measured with radiation detec-
 86 tors arranged around the BPT as shown in Fig. 1. Two
 87 plastic-scintillator ΔE - E telescopes, two microchan-
 88 nnel-plate (MCP) detectors, and two high-purity germanium
 89 (HPGe) detectors are used to measure β particles, recoil
 90 ions, and γ rays, respectively.

91 Beta-delayed-neutron spectroscopy is performed by
 92 recording the time of flight (TOF) of the recoil ions,
 93 which is determined from the time difference between
 94 the β particle hitting a ΔE detector and the recoil ion
 95 hitting an MCP detector. Due to the additional momen-
 96 tum imparted by the neutron, ions from βn emission
 97 have shorter TOFs than those from β decay without neu-
 98 tron emission. The recoil-ion momentum can be recon-
 99 structed from the TOF and the distance the ion trav-
 100 els to the MCP surface. The neutron energy may then
 101 be obtained through conservation of energy and momen-
 102 tum. The resulting neutron-energy spectrum can be deter-
 103 mined down to 100 keV; at lower energies, TOF cannot
 104 be used to identify βn events because the corresponding
 105 recoil ions have energies comparable to those from β
 106 decays without neutron emission. In this section, the ion
 107 production, transport, and confinement, as well as the
 108 detection of the decay particles are discussed.

109 A. Beam delivery at CARIBU

110 At CARIBU, fission fragments from a $\sim 100\text{-mCi}$ ^{252}Cf
 111 source were thermalized in a large helium-filled gas
 112 catcher [20], extracted primarily as 1^+ ions, transported
 113 through an isobar separator [23], and delivered to a
 114 radiofrequency-quadrupole buncher containing a small
 115 amount of helium gas to accumulate, cool, and bunch
 116 the beam. The isobar separator had a mass resolution
 117 of $M/\Delta M \approx 14000$, which allowed for some suppression
 118 of the two neighboring isobars and essentially complete
 119 removal of all other isobars.

120 The optimal isobar-separator settings were selected by
 121 monitoring the distribution of isotopes present in the
 122 beam during tuning. The beam composition was charac-

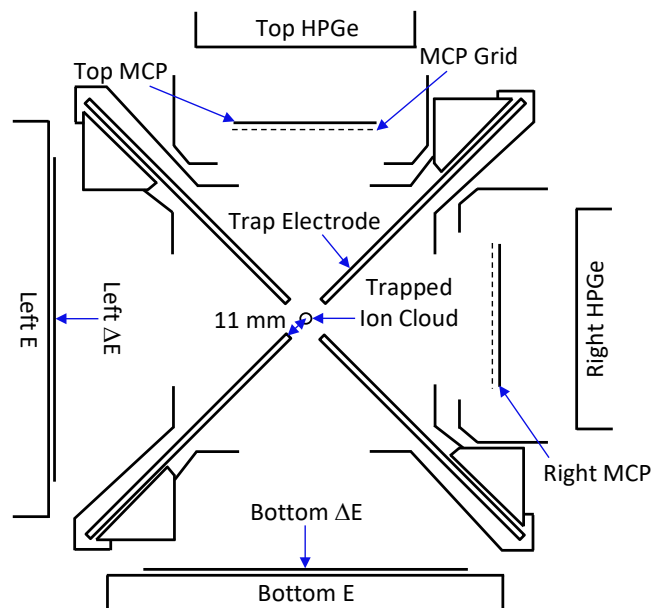


FIG. 1. (Color online) Cross-sectional view of the BPT and detectors used in the experiment (not to scale); the beam axis points perpendicularly into the plane. The detectors are labeled by their orientation relative to the beam direction at the center of the trap. Two plastic ΔE - E telescopes, two MCP detectors, and two HPGe detectors were used to measure β particles, recoil ions, and γ rays, respectively. Four sets of electrode plates were used to confine ions in the trap. Each plate came within 11 mm of the center of the BPT.

123 terized by using the two HPGe detectors surrounding the
 124 BPT and by performing mass scans with the Canadian
 125 Penning Trap (CPT) mass spectrometer [24, 25]. The
 126 ion bunches were injected into the BPT at time inter-
 127 vals of t_{int} and accumulated over a length of time t_{meas} ,
 128 after which the ions were ejected from the trap to mea-
 129 sure backgrounds over a time period t_{bkgd} ; this cycle was
 130 repeated throughout the entire run. The values of t_{int} ,
 131 t_{meas} , and t_{bkgd} used for each isotope are given in Ta-
 132 ble I and were chosen based on the radioactive half-life of
 133 the isotope being studied and the distribution of isobaric
 134 contaminants present during the measurement. The total
 135 measurement times and average beam rates are also
 136 shown in Table I.

137 B. Trapping with the BPT

138 Ion confinement was achieved by applying direct-
 139 current (DC) and time-varying, sinusoidal radiofre-
 140 quency (RF) voltages to four sets of electrode plates ex-
 141 tending to within 11 mm from the center of the trap as
 142 shown in Fig. 1. The DC voltages were used to produce
 143 a harmonic confining potential with a $\sim 5\text{-V}$ electrostatic
 144 valley in the axial direction, and the RF voltages, with a
 145 peak-to-peak amplitude of about 200 V and a frequency

TABLE I. The measurement time, average beam rate, and trapping-cycle information (t_{int} , t_{meas} , t_{bkgd}) for the measurements. During each measurement cycle, ion bunches were injected into the BPT at time intervals of t_{int} , accumulated over a length of time t_{meas} , then ejected from the BPT for a background measurement lasting t_{bkgd} .

Isotope	Half-life (s)	Measurement time (h)	Average beam rate (ions/s)	t_{int} (s)	t_{meas} (s)	t_{bkgd} (s)
^{135}Sb	1.679(15) [26]	45.7	50	1.0	19.9	10.1
^{136}Sb	0.923(14) [27]	60.7	5	0.6	8.9	4.9
^{140}I	0.86(4) [28]	35.3	5	0.6	8.3	4.3

of 310 kHz, were used to confine ions in the radial direction. Higher harmonics at 620 and 930 kHz were observed with amplitudes less than 10% of the amplitude of the primary frequency. The trapped ions were thermalized in $\sim 5 \times 10^{-5}$ Torr of helium gas.

Following β decay, the charge state of the recoil ion is typically 2^+ ; however, higher charge states can arise due to processes such as electron shakeoff, Auger-electron emission, and internal conversion. The stability conditions for the BPT, determined from the Mathieu equations [29], were chosen so that the decay daughters, which all have charge states higher than 1^+ , were not confined in the trap.

C. Particle detection

Two plastic-scintillator ΔE - E telescopes were used for β spectroscopy. The ΔE detector was a 1-mm-thick, 10.6-cm-diameter disk that had a nearly 100% intrinsic detection efficiency for β particles and only a $\sim 1\%$ intrinsic detection efficiency for γ rays and neutrons. The ΔE detectors were placed ~ 105 mm from the center of the BPT and each covered a solid angle of 5% of 4π . The E detectors were 10.2-cm-thick, 13.3-cm-diameter disks located immediately behind the ΔE detectors that were capable of stopping the β particles. Each ΔE - E telescope was contained in its own vacuum chamber (held below 10^{-3} Torr) and separated from the BPT vacuum by a 10- μm -thick aluminized-Kapton window. The Left and Bottom ΔE detectors had β -energy thresholds of 76(24) keV and 62(30) keV, respectively, and a neutron detection threshold of 370(70) keV [21].

Two 50.3×50.3 mm² resistive-anode Chevron MCP detectors [30] with 1-ns timing resolution and sub-mm position sensitivity were used for recoil-ion detection. The front face of each detector was biased to approximately -2.5 kV to accelerate incoming ions and thereby provide a more uniform detection efficiency. Each detector was placed 4.5 mm behind a grounded 89%-transmission grid to help shield the detector from the RF fields of the BPT and to prevent the recoil-ion trajectories from being affected by the MCP bias voltage until they passed through the grid. The hit locations of the ions were reconstructed from the relative amounts of charge collected at the four corners of the anode [31]. The central 46×46 mm² region of each MCP detector had

the best position resolution and was taken to be the fiducial area in the data analysis. Each detector was located 53.0(5) mm away from the trap center and subtended a solid-angle of 5% of 4π .

The intrinsic efficiencies of the MCP detectors were determined to be 33.3(15)% and 29.3(14)% for the Right and Top detectors, respectively, from a detailed study of the decays of trapped ^{134}Sb ions held in the BPT [32]. The ion detection efficiencies also had to be corrected for additional loss of MCP pulses to electronic thresholds [21, 33]. For the Right MCP detector, this was a $<3\%$ correction. However, the Top MCP detector had a lower gain, resulting in a correction that ranged between ~ 5 –30% (depending on the impact energy of the ions) and showed some spatial dependence.

Two coaxial single-crystal p-type HPGe detectors were used to detect γ rays. The detectors, which had relative efficiencies of 80% and 140%, were located within 10 cm of the trapped-ion cloud behind the Right and Top MCP detectors, respectively. Standard γ -ray point sources (^{60}Co , ^{133}Ba , ^{137}Cs , ^{152}Eu) with activities determined to within 1.5–2.5% (at 1σ) were used to calibrate the photopeak detection efficiencies.

The data-acquisition system was triggered on a signal from any detector. A 22- μs coincidence window was then opened, during which the amplitude and timing of each detected event was recorded along with the phase of the BPT RF voltage. The TOF for recoil ions was determined with a timing resolution of 3 ns FWHM. The nonparalyzable deadtime per event was 142 μs .

III. ANALYSIS AND RESULTS

The TOF of the recoil ions was determined from ΔE -MCP detector coincidences and used to distinguish βn decays from β decays without neutron emission. The TOF spectra measured for $^{135,136}\text{Sb}$ and ^{140}I are shown in Fig. 2. The βn events have TOFs primarily between 200 and 2000 ns, and β -decay events without neutron emission have longer TOFs. A peak at 0 ns arose from electron events in the ΔE detector that were in coincidence with a γ ray or scattered electron triggering the MCP detector.

The βn energy spectra and branching ratios determined from these TOF spectra are discussed in this section. The Monte Carlo simulations of the decays and

234 experimental setup needed to analyze the data are intro-
 235 duced first.

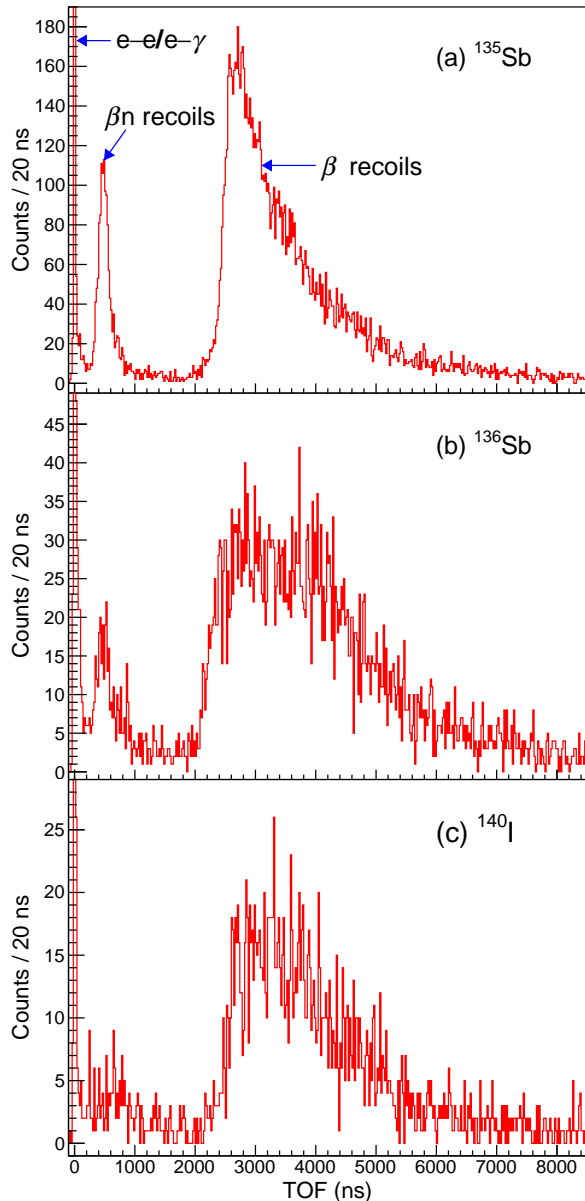


FIG. 2. (Color online) TOF spectra for (a) ^{135}Sb , (b) ^{136}Sb , and (c) ^{140}I . Events between 200 and 2000 ns are primarily due to recoil ions from βn decay, and events above 2000 ns are primarily due to recoil ions from β decay without neutron emission. The peak at 0 ns is due to coincidences where an electron hit a ΔE detector and a γ ray or scattered electron triggered an MCP detector.

A. Monte Carlo simulations

237 The β -decay kinematics were generated using simu-
 238 lation code originally developed in Ref. [34] and later

239 adapted for βn decay [17, 32, 35]. For each β -decay tran-
 240 sition, a distribution of β and $\bar{\nu}$ momenta was generated,
 241 assuming an allowed β -spectrum shape. For transitions
 242 to excited states in the daughter nucleus, the subsequent
 243 deexcitation by the emission of γ rays, conversion elec-
 244 trons (CEs), and neutrons was also included. The result-
 245 ing nuclear recoil was determined from the momentum
 246 imparted from each of these decay particles.

247 For βn emission, the transitions were assumed to be
 248 allowed Gamow-Teller, which results in a β -decay rate of
 249 the form [36]

$$W \propto F(Z, E_e) p_e E_e (E_0 - E_e)^2 \left[1 + a_{\beta\bar{\nu}} \frac{\vec{p}_e \cdot \vec{p}_{\bar{\nu}}}{E_e E_{\bar{\nu}}} + a_{\beta\nu n} \left(\frac{(\vec{p}_e \cdot \hat{n})(\vec{p}_{\bar{\nu}} \cdot \hat{n})}{E_e E_{\bar{\nu}}} - \frac{1}{3} \frac{\vec{p}_e \cdot \vec{p}_{\bar{\nu}}}{E_e E_{\bar{\nu}}} \right) \right], \quad (1)$$

250 where $F(Z, E_e)$ is the Fermi function, (E_e, \vec{p}_e) and
 251 $(E_{\bar{\nu}}, \vec{p}_{\bar{\nu}})$ are the β and $\bar{\nu}$ four-momenta respectively, E_0 is
 252 the β end-point energy, and \hat{n} is the neutron-momentum
 253 unit vector. The parameter $a_{\beta\bar{\nu}}$ is the β - $\bar{\nu}$ angular cor-
 254 relation and is equal to $-1/3$ for allowed Gamow-Teller
 255 decays. The parameter $a_{\beta\nu n}$ is referred to here as the β -
 256 $\bar{\nu}$ -neutron “triple correlation,” and its size depends on the
 257 spins of the parent, daughter, and granddaughter states
 258 populated in the decay. A range of $a_{\beta\nu n}$ coefficients had
 259 to be considered for the three isotopes of interest because
 260 several spin sequences are accessible via allowed β decay.
 261 In addition, for the βn decay of ^{135}Sb , neutron emis-
 262 sion to a few low-lying excited states in ^{134}Te , which had
 263 previously been observed [37], were considered as well.
 264 For ^{136}Sb and ^{140}I , only βn decays to the ground states
 265 of ^{135}Te and ^{139}Xe , respectively, were assumed, as there
 266 are no data indicating population of excited states.

267 For transitions to states in the daughter nucleus be-
 268 low the neutron-separation energy, an approximation was
 269 made that for a given isotope, all the $a_{\beta\bar{\nu}}$ were fixed to
 270 a single value, which was determined from the measured
 271 β -ion coincidences using an approach described in detail
 272 in Ref. [35]. For ^{135}Sb and ^{140}I , this value of $a_{\beta\bar{\nu}}$ was
 273 $+0.23$ and -0.42 , respectively. For ^{136}Sb , the presence
 274 of trapped ^{136}Te ions complicated the analysis of the re-
 275 coil ions and a value for $a_{\beta\bar{\nu}}$ could not be obtained.

276 The β decays were spatially distributed with a 1-mm-
 277 FWHM Gaussian distribution in three dimensions, cor-
 278 responding to the measured ion-cloud extent [32]. The
 279 emitted β particles, γ rays, CEs, and neutrons were prop-
 280 agated using GEometry ANd Tracking 4 (GEANT4) [38,
 281 39] version 4.10.0.p01 to model the scattering and en-
 282 ergy loss of the particles within the apparatus. The en-
 283 ergies deposited in the ΔE , E , and HPGe detectors were
 284 recorded, and the electronic thresholds of the ΔE de-
 285 tectors were taken into account. Recoil ions of various
 286 charge states were propagated through the time-varying
 287 electric fields of the BPT using the SIMION 8.1 [40] ion-
 288 optics code. The average charge states following the de-
 289 cay of $^{135,136}\text{Sb}$ and ^{140}I were determined to be 2.20, 2.51,

290 and 2.16, respectively [35], from the RF-phase depen- 315
 291 dence of the measured β -ion coincidence rate using the 316
 292 approaches described in Ref. [32]. For ions that struck 317
 293 an MCP detector, a threshold cut was applied [21] and 318
 294 the TOF, energy, and position at impact were recorded.

295 The efficiencies for detecting β particles and β -ion 319
 296 coincidences were determined using these simulations. 320
 297 Fig. 3 shows the β -ion-coincidence detection efficiency 321
 298 as a function of neutron energy for ^{135}Sb , with the prod- 322
 299 uct of the corresponding detector solid angles and MCP- 323
 300 detector intrinsic efficiency divided out. At the high- 324
 301 est neutron energies, the coincidence-detection efficiency 325
 302 drops rapidly because of the limited energy available for 326
 303 the leptons, which results in fewer β particles having en- 327
 304 ergies above the ΔE detector thresholds. However, β de- 328
 305 cays that populate highly-excited states are largely sup- 329
 306 pressed because of phase-space considerations. The two 330
 307 180° combinations (Left-Right and Bottom-Top) have 331
 308 higher efficiencies than the two 90° combinations (Left- 332
 309 Top and Bottom-Right) primarily because of neutron-ion 333
 310 coincidences, which are present because the neutron and 334
 311 recoil ion are emitted with momenta nearly 180° apart 335
 312 and therefore strike back-to-back detectors. The β -ion- 336
 313 coincidence detection-efficiency curves for ^{136}Sb and ^{140}I 337
 314 have similar features.

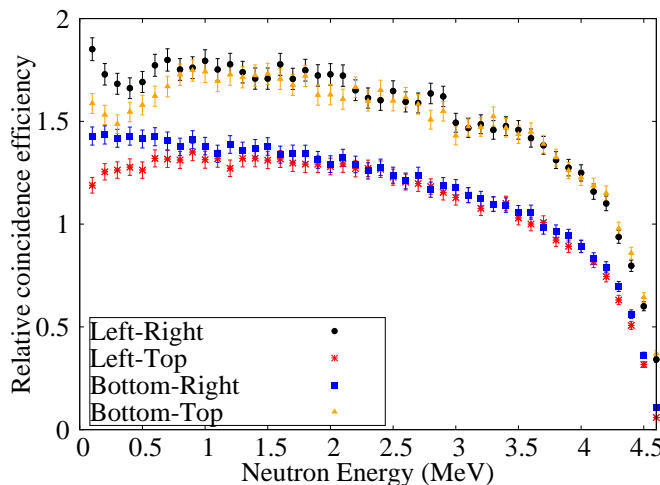


FIG. 3. (Color online) The β -ion-coincidence detection effi-
 ciency for each ΔE -MCP detector pair as a function of neu-
 tron energy for ^{135}Sb ; the product of the corresponding de-
 tector solid angles and MCP-detector intrinsic efficiency has
 been divided out. The two 180° combinations (Left-Right
 and Bottom-Top) have higher efficiencies than the two 90°
 combinations (Left-Top and Bottom-Right) primarily because
 of additional events from neutron-ion coincidences. At the
 highest neutron energies, the coincidence detection efficiency
 drops rapidly because of the limited energy available for the
 leptons; however, few β decays are expected to yield neu-
 trons at these energies because of phase-space considerations.
 The β -ion-coincidence detection-efficiency curves for ^{136}Sb
 and ^{140}I have similar features.

B. Neutron energy spectra

316 The neutron energy was obtained by assuming the re-
 317 coil ion and neutron had equal and opposite momenta.
 318 The recoil-ion momentum was determined from the ion
 319 TOF and hit position on the MCP surface; the distance
 320 traveled by the ion was approximated as a straight path
 321 from the trap center to the MCP grid, and effects due
 322 to the electric field between the grid and the MCP sur-
 323 face were handled analytically. Background events were
 324 then subtracted, corrections were made to account for
 325 the contribution to the recoil-ion momentum from lep-
 326 ton emission, and the spectrum was scaled by the β -ion
 327 coincidence efficiency. Each of these data-analysis steps
 328 is explained below.

329 The background from accidental coincidences was de-
 330 termined from the TOF region between 15–20 μs , which
 331 both data and simulation indicated had no true β -ion
 332 coincidences. This subtraction resulted in a 3–9% cor-
 333 rection, depending on the isotope.

334 After accounting for accidental coincidences, counts re-
 335 mained in the 50–200-ns time window where no β -ion
 336 coincidences from trapped ions were expected. These
 337 counts were present both while the BPT was trapping
 338 ions and while the BPT was held empty following ejection
 339 of the trapped ions and were likely due to radioactiv-
 340 ity that accumulated on the BPT and detector surfaces
 341 during data collection. The TOF distribution of these
 342 events was most pronounced between 50–200 ns and de-
 343 creased with increasing TOF, extending into the βn TOF
 344 region. The shape of this background, when converted
 345 into a neutron-energy distribution, closely resembled an
 346 exponential function. The subtraction of this background
 347 was performed by normalizing this exponential function
 348 to match the number of counts between 50–200 ns col-
 349 lected when the BPT was trapping ions. This resulted in
 350 a 15–30% correction to the total number of observed βn
 351 decays, depending on the isotope being analyzed.

352 Following background subtraction, the neutron-energy
 353 spectrum was adjusted to account for the momentum im-
 354 parted to the recoil ion from lepton emission. For the
 355 β -ion coincidences measured by detectors 90° apart, this
 356 effect was small — it resulted in energy shifts of up to
 357 1–2% for all neutron energies and was impacted negligi-
 358 bly by the triple correlation and the population of any
 359 excited states following neutron emission. For the β -ion
 360 coincidences measured by detectors 180° apart, the neu-
 361 tron energy tended to be overestimated because the β
 362 particle was emitted in approximately the same direc-
 363 tion as the neutron and therefore contributed to the mo-
 364 mentum of the nuclear recoil. The size of the energy
 365 shift is influenced by the β - $\bar{\nu}$ angular correlation $a_{\beta\nu}$ and
 366 the triple correlation $a_{\beta\nu n}$. When considering only $a_{\beta\nu}$,
 367 simulations showed that neglecting the leptons would re-
 368 sult in an overestimation of the inferred neutron energy
 369 of 25–30% at 100 keV, which steadily decreases to 10%,
 370 7%, and less than 4% at neutron energies of 500 keV,
 371 1000 keV, and above 2000 keV, respectively. The impact

of $a_{\beta\nu n}$ on the energy shift is much smaller by comparison. For each isotope, there are a number of possible triple-correlation coefficients due to the various parent-daughter-granddaughter spin sequences accessible by allowed β decay. Transitions with the lowest possible orbital angular momentum, L , for neutron emission (yielding $L = 2$ for all three isotopes) were assumed to dominate the βn decays. For ^{135}Sb , only one possible spin sequence results in $L = 2$, and that gives $a_{\beta\nu n} = 0.286$. For ^{136}Sb and ^{140}I , there are three spin sequences, which lead to values for $a_{\beta\nu n}$ of -0.571 , -0.143 , 0.286 and -0.786 , 0.071 , 0.286 , respectively. For ^{136}Sb and ^{140}I , the average of these correlation coefficients was used, which had the effect of increasing the inferred neutron energies by less than 1%. The spread in $a_{\beta\nu n}$ resulted in an uncertainty in the neutron energy of about 2.5% at 100 keV, which fell to $< 1\%$ by 600 keV. For ^{135}Sb , the triple correlation resulted in a 1.5% decrease in the neutron energy at 100 keV and a $< 1\%$ decrease above 300 keV. In addition, the inclusion of transitions to the first, second, and third excited states in ^{134}Te (populated with probabilities of 21%, 11%, and 6%, respectively [37]) also influenced the size of the energy shift due to lepton (and subsequent γ -ray) emission. Accounting for excited states resulted in an increase in the neutron energy that was 3% at 100 keV and fell to $< 1\%$ above 1300 keV.

For each isotope, the neutron-energy spectrum obtained for each ΔE -MCP detector pair was corrected by the corresponding neutron-energy-dependent β -ion coincidence efficiency, and the results were summed together. As a final step, the contribution from isobaric contaminants in the ion cloud was subtracted. During data collection, neighboring isobars were suppressed but not completely removed. For $^{135,136}\text{Sb}$ and ^{140}I , the more neutron-rich isobar ($^{135,136}\text{Sn}$ and ^{140}Te , respectively) is a βn emitter, but has a ^{252}Cf -fission yield a couple orders of magnitude lower than the isotope of interest, making its contribution to the total number of βn decays in the BPT negligible. For ^{135}Sb and ^{140}I , the more proton-rich isobar (^{135}Te and ^{140}Xe , respectively) does not decay by βn emission and therefore cannot contribute βn events. For ^{136}Sb , the more proton-rich isobar, ^{136}Te , has a βn branching ratio roughly ten times smaller than that of ^{136}Sb , but a fission yield 30 times larger. The suppression of ^{136}Te by the isobar separator, together with the measurement cycle favoring the shorter-lived species, resulted in an average trapped-ion activity with about 10–15% more ^{136}Sb than ^{136}Te . The ^{136}Te contribution to the total number of βn coincidences was determined to be 5% based on the ratio of the ^{136}Sb and ^{136}Te activities, after accounting for the βn branching ratios and the fraction of neutrons with energies above the 100-keV neutron threshold (estimated to be 0.6(2) for ^{136}Te from the neutron-energy spectrum in Ref. [41] and determined in Sec. III C to be 0.89(6) for ^{136}Sb). For the ^{136}Sb neutron-energy spectrum, the contribution from ^{136}Te isobaric contamination was removed by subtracting the ^{136}Te neutron-energy spectrum measured in

Ref. [41], which was scaled by the activity and βn branching ratio and broadened to account for the experimental energy resolution.

The neutron-energy resolution in the present work was primarily determined by the spatial distribution of the ion cloud and the spread in recoil momentum resulting from the lepton emission. The 1-mm width of the ion cloud resulted in a 4%-FWHM energy resolution, regardless of neutron energy. With lepton emission included, simulations indicated that the FWHM energy resolution was 60% at a neutron energy of 100 keV and steadily decreased to 25%, 15%, and 9% at 500 keV, 1000 keV, and above 2000 keV, respectively. The neutron energy spectrum was determined down to 100 keV; below this energy, the recoil momentum imparted from the emission of the leptons and any accompanying γ rays was comparable to the momentum imparted from neutron emission.

The βn -energy spectra obtained in the present work for $^{135,136}\text{Sb}$ and ^{140}I are shown in Fig. 4. For ^{135}Sb and ^{140}I , the spectra are compared with direct neutron measurements by Kratz *et al.* [14] and Shalev and Rudstam [42], respectively. For ^{136}Sb , no previous measurement of the energy spectrum has been made. In the experiment by Kratz *et al.*, βn precursors were produced through neutron-induced fission of ^{235}U at the Mainz TRIGA reactor, and two ^3He ionization chambers, with energy resolutions of 12 keV for thermal neutrons and 20 keV for 1-MeV neutrons, were used to measure neutron energies. In the experiment by Shalev and Rudstam, βn precursors were produced at the OSIRIS isotope-separator on-line facility. Neutron energies were measured with a neutron spectrometer that consisted of a cylindrical gridded ionization chamber filled with a ^3He -argon gas mixture. The results obtained with the BPT for ^{135}Sb and ^{140}I have neutron-energy spectra and energy thresholds that are similar to the direct measurements. For ^{135}Sb , the peaks in the spectrum obtained here are not as sharp because of the wider energy resolution.

The uncertainty in the energy scale for the data collected with the 90° detector pairs was about 2% and was due largely to the uncertainty in the distance between the trap center and the MCP detector face. This distance was determined to about 1% precision from measurements of the trap-electrode and detector locations and an analysis of the recoil-ion TOF spectra [32]. For the 180° pair, the energy-scale uncertainties were larger: 3% at 100 keV, with a decrease back down to 2% by 1000 keV. This increase was due primarily to the spread in the potential size of the neutron-energy correction related to lepton emission.

C. βn branching ratios

The βn branching ratios were obtained by comparing the number of detected β -ion coincidences corresponding to decays that emitted a neutron with energy above 100 keV, $n_{\beta R}$, to the number of detected β particles, n_{β} ,

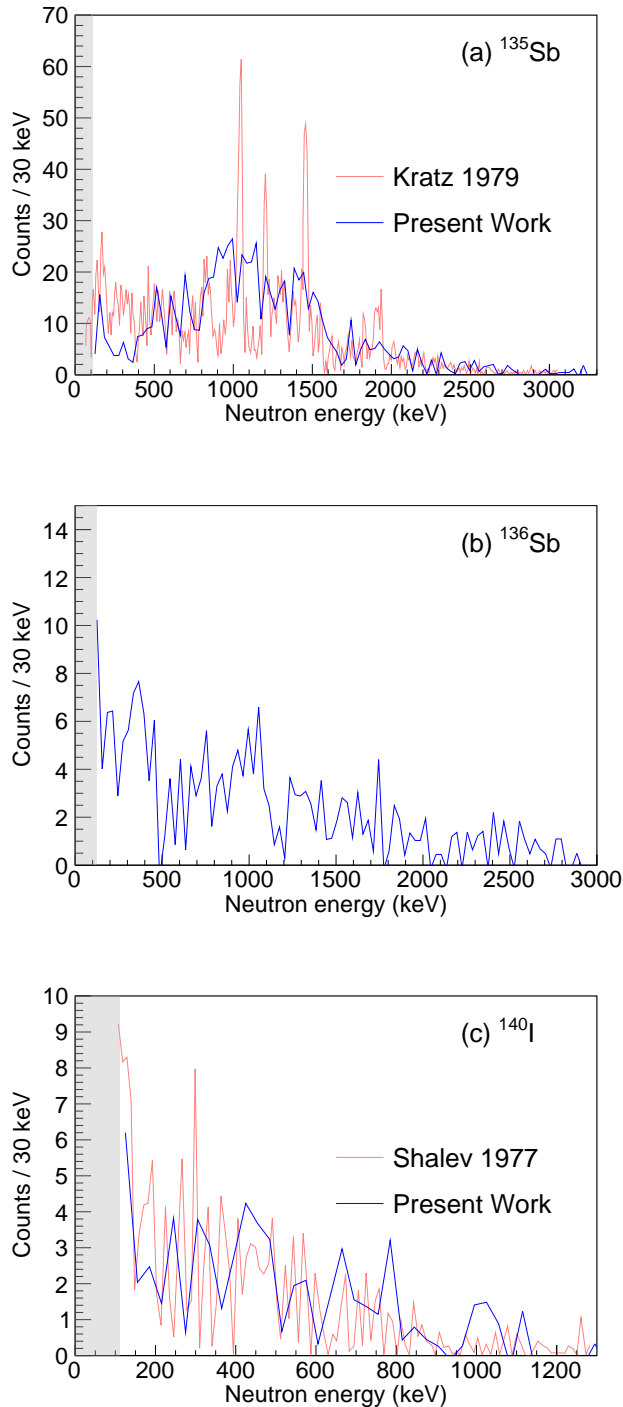


FIG. 4. (Color online) Neutron energy spectra for (a) ^{135}Sb , (b) ^{136}Sb , and (c) ^{140}I compared with results from Kratz *et al.* [14] and Shalev and Rudstam [42]. The y-axis label refers to the present work, where each data point corresponds to a 30-keV-wide bin. For the ^{135}Sb spectrum measured by Kratz *et al.* and the ^{140}I spectrum measured by Shalev and Rudstam, the data points correspond to 8-keV-wide and 10.75-keV-wide bins, respectively. In the gray region below 100 keV, no neutron-energy information was obtained in the present work because the TOF of recoils from βn emission could not be distinguished from those from β decay without neutron emission.

through the relation

$$P_n = \frac{n_{\beta R}/(\epsilon_{\beta R} \cdot f)}{n_{\beta}/\epsilon_{\beta}}, \quad (2)$$

where $\epsilon_{\beta R}$ is the efficiency for detecting the β -ion coincidences and ϵ_{β} is the β -particle detection efficiency. The ratio $\epsilon_{\beta}/\epsilon_{\beta R}$ was determined from the Monte Carlo simulations discussed in Sec. III A and the value of the intrinsic MCP efficiency obtained in Ref. [32]. The uncertainty in the ratio was 7%, with the largest contributions being from the detector thresholds, the treatment of β scattering, and the intrinsic MCP efficiency.

The parameter f is the fraction of the total βn spectrum that lies above the experimental threshold of 100 keV. As there is either little or no information on the region below 100 keV for the three isotopes studied here, an assumption had to be made about this portion of the spectrum. It was assumed that the energy spectrum did not vary dramatically at low energies and therefore, the measured neutron intensity between 100–200 keV could be used as an estimate of the unobserved neutron intensity from 0–100 keV. Values of 0.95(3), 0.89(6), and 0.83(9) were obtained for $^{135,136}\text{Sb}$ and ^{140}I , respectively, where the uncertainty was set to half the difference from unity to allow for possible structure in the spectra below 100 keV.

To determine n_{β} , the ΔE triggers originating from the trapped species of interest were isolated from those due to decays of isobaric contaminants and other backgrounds. This was accomplished by comparing the data to a model that takes into account the buildup and decay of the different species in the BPT over the course of the trapping cycle, while enforcing the decay-feeding relationships between the different populations [43]. For ^{135}Sb , ^{136}Sb , and ^{140}I , n_{β} was obtained with 7%, 8%, and 12% precision respectively.

For ^{135}Sb and ^{140}I , the βn branching ratio was also obtained directly from the recoil-ion TOF spectrum by comparing $n_{\beta R}$ to the number of β -ion coincidences observed for decays without neutron emission, $n_{\beta r}$, using

$$P_n = \frac{n_{\beta R}/(\epsilon_{\beta R} \cdot f)}{n_{\beta R}/(\epsilon_{\beta R} \cdot f) + n_{\beta r}/\epsilon_{\beta r}}, \quad (3)$$

where $\epsilon_{\beta r}$ is the efficiency for detecting β -ion coincidences for decays without neutron emission and was determined in Ref. [35] from Monte Carlo simulations. The efficiency $\epsilon_{\beta r}$ is sensitive to the details of the decay scheme and the charge-state distribution of the recoil ions following β decay. Information on the decay scheme is typically either incomplete or unavailable. However, Ref. [35] demonstrated that $\epsilon_{\beta r}$ could be obtained with a precision of 4% by adjusting various decay-scheme parameters until the results of the simulation matched both the measured energy deposition in the plastic E detector and the ratio of β -ion coincidences obtained from detectors 180°

TABLE II. Recommended βn branching ratios obtained in the present work. Uncertainties are divided into statistical and systematic.

Isotope	P_n (%)
^{135}Sb	14.6 ± 0.4 (stat) ± 1.2 (sys)
^{136}Sb	17.6 ± 1.0 (stat) ± 2.7 (sys)
^{140}I	7.6 ± 0.9 (stat) ± 2.7 (sys)

and 90° apart. The adjusted parameters included an $a_{\beta\nu}$ coefficient common to all transitions and a distribution of β -decay intensities to excited states in the daughter nucleus. The ratio $\epsilon_{\beta R}/\epsilon_{\beta r}$ was determined with a total uncertainty of 7%, which was primarily due to the detector thresholds, simulation of β -scattering, the intrinsic MCP efficiency, and limited information on the β -decay pattern.

The value of $n_{\beta r}$ was obtained by summing the number of coincident events in the TOF region where β decays without neutron emission are expected and subtracting the contribution from isobaric contaminants (if present) and accidental coincidences. For ^{135}Sb and ^{140}I , $n_{\beta r}$ was determined with 3% and 6% precision, respectively. For ^{136}Sb , the trapped ^{136}Te activity was substantial enough that a reliable subtraction of its contribution was not possible.

The βn branching ratios were obtained from the weighted average of the results from the four ΔE -MCP detector pairs. For ^{135}Sb and ^{140}I , P_n values of 14.7(18)% and 8.1(35)%, respectively, were determined from Eq. 2, and values of 14.6(13)% and 7.6(28)%, respectively, were determined from Eq. 3. For ^{136}Sb , Eq. 2 yielded a P_n of 17.6(29)%. In these approaches to determining P_n , the systematic uncertainty due to the β -particle detection efficiency largely cancels out. However, obtaining P_n directly from the recoil-ion TOF spectrum yields a smaller total uncertainty because the systematic uncertainties due to the MCP solid angles and intrinsic efficiencies also cancel out. Therefore, for ^{135}Sb and ^{140}I , the βn branching ratios obtained from the recoil-ion TOF spectrum are recommended; for ^{136}Sb , only the P_n value obtained from the comparison to detected β particles is available. In Table II, the recommended βn branching-ratio results are provided. These values are compared with results obtained from previous direct measurements in Fig. 5. In the direct measurements, P_n was determined either from the fission yield and neutrons-per-fission of the isotope [44–49], or by counting β particles and neutrons separately [50–54], usually with plastic scintillators and neutron detectors (e.g., BF_3 tubes, ^3He tubes), respectively. For each isotope, there is roughly a factor of two spread among the P_n results, despite the fact that in many cases, the quoted uncertainties are significantly smaller than these differences. These discrepancies are evident even when comparing measurements that used similar experimental techniques, underscoring the challenging nature of performing βn spectroscopy and indi-

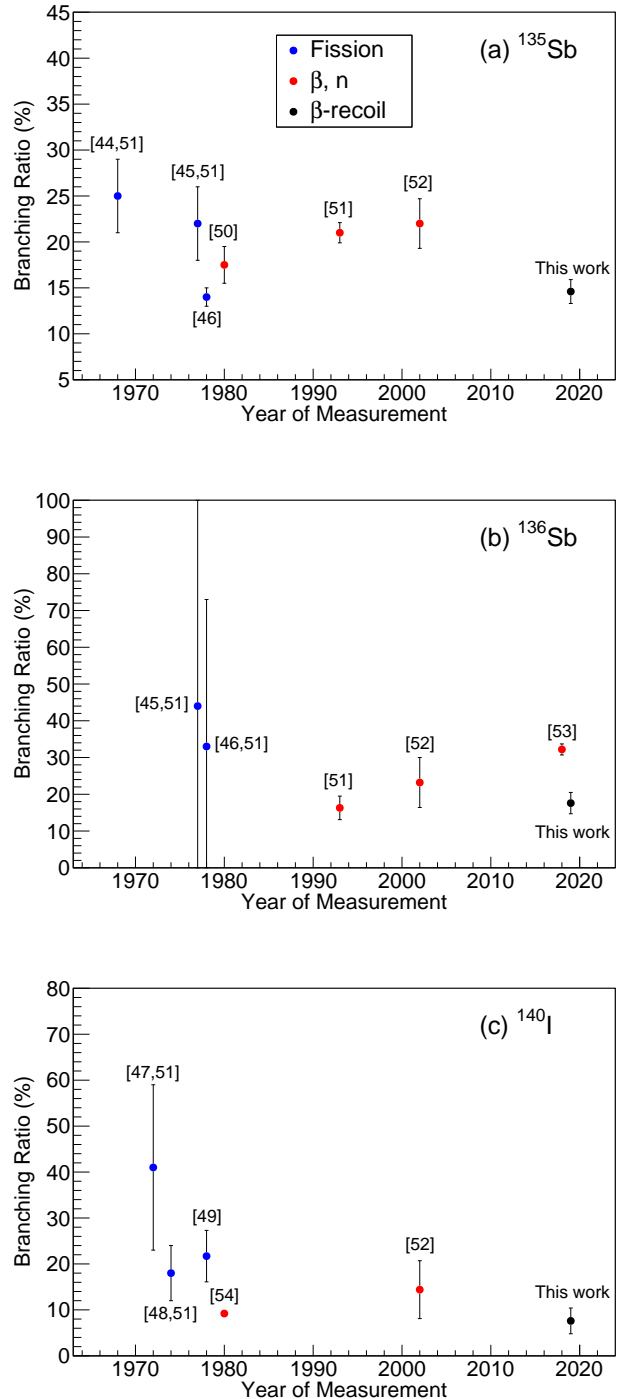


FIG. 5. (Color online) Beta-delayed-neutron branching ratios from the present work (values taken from Table II) compared with previous direct measurements for (a) ^{135}Sb , (b) ^{136}Sb , and (c) ^{140}I . The corresponding year, reference(s), and measurement technique are provided for each measurement. The label “fission” indicates that P_n was obtained from the fission yield and neutrons-per-fission of the isotope. “ β, n ” indicates that P_n was obtained by counting β particles and neutrons separately, usually with plastic scintillators and neutron detectors (e.g., BF_3 tubes, ^3He tubes), respectively, and “ β -recoil” refers to the present work.

582 cating unforeseen systematic effects were likely responsi- 633
583 ble for these differences.

584 The P_n results for $^{135,136}\text{Sb}$ and ^{140}I were determined 634
585 in an analogous manner to the results for $^{137,138}\text{I}$ and 635
586 $^{144,145}\text{Cs}$ in Ref. [21]. In Ref. [21], the βn branching ratios 636
587 were obtained by comparing the number of β -ion coinci- 637
588 dences corresponding to βn decay to the β -decay activity, 638
589 which was measured three different ways: (1) from the 639
590 number of β particles detected by the ΔE detectors, (2) 640
591 from the number of β -ion coincidences registered by the 641
592 ΔE and MCP detectors, and (3) from the number of β - γ 642
593 coincidences registered by the ΔE and HPGe detectors. 643
594 These three independent measures gave consistent P_n re- 644
595 sults that were in excellent agreement with previous di- 645
596 rect measurements. They also presented an opportunity 646
597 to probe systematic effects and provided confidence that 647
598 they were under control. In the present work, P_n was ob- 648
599 tained using methods (1) and (2), with limited statistics 649
600 for β -delayed γ -ray emission not allowing method (3). 650
601 For ^{135}Sb and ^{140}I , where P_n from methods (1) and (2) 651
602 could be compared, consistent results were obtained. 652

603 IV. SUMMARY AND CONCLUSIONS

604 Beta-delayed-neutron spectroscopy was performed us- 653
605 ing the BPT instrumented with two plastic-scintillator 654
606 ΔE - E telescopes, two MCP detectors, and two HPGe 655
607 detectors to measure β particles, recoil ions, and γ rays, 656
608 respectively. Both the βn energy spectra and branch- 657
609 ing ratios were determined for the neutron-rich nuclei 658
610 $^{135,136}\text{Sb}$ and ^{140}I . The βn energy spectrum for ^{136}Sb 659
611 was measured for the first time, and the spectra for ^{135}Sb 660
612 and ^{140}I were compared with results from direct neutron 661
613 measurements by Kratz *et al.* [14] and Shalev and Rud- 662
614 stam [42], respectively. The βn energy spectra from the 663
615 present work were similar in shape and had comparable 664
616 energy thresholds to those obtained through direct neu- 665
617 tron detection. 666

618 The βn branching ratios were obtained by comparing 670
619 the number of β -ion coincidences from βn decays to the 671
620 number of detected β decays, which was determined from 672
621 the number of β particles registered by the ΔE detector 673
622 and, when possible, the number of β -ion coincidences. 674
623 The latter approach to determining the number of de- 675
624 tected β decays was preferred when available, as it re- 676
625 sulted in smaller systematic uncertainties in P_n . 677

626 $^{135,136}\text{Sb}$ and ^{140}I fall within a neutron-rich region of 678
627 the nuclear chart where βn emission can significantly im- 679
628 pact the r -process abundance pattern around the $A \approx$ 680
629 130 mass peak. During r -process nucleosynthesis, βn 681
630 emission shifts isotopes along mass chains while decays 682
631 back to stability occur, and the released neutrons are 683
632 available for additional late-time, non-equilibrium cap-

633 tures [4, 22, 55]. The βn branching ratios obtained in this
634 work for $^{135,136}\text{Sb}$ and ^{140}I were found to be smaller than
635 those of most previous measurements. If other isotopes
636 in this vicinity also have smaller βn branching ratios than
637 currently predicted, the influence of this decay process on
638 the r -process abundance pattern would be reduced.

639 The neutron-energy spectra were obtained with β -ion-
640 coincidence efficiencies of $\sim 0.5\%$, which is several orders
641 of magnitude larger than the neutron-detection efficien-
642 cies achievable with the ^3He and gas-proportional detec-
643 tors used for direct neutron spectroscopy. The ion-trap
644 approach is therefore well suited for use at radioactive-
645 beam facilities, where efficient techniques are desired to
646 make the most of the delivered beam intensities. The
647 βn branching ratios for ^{136}Sb and ^{140}I were determined
648 with beam intensities of only 5 ions/s, and with improve-
649 ments to the detector array, results could be obtained
650 with beams of less than 1 ion/s.

651 Upgrades to the BPT setup are currently in develop-
652 ment. Plans include increasing the β -recoil-coincidence
653 detection efficiency using larger plastic scintillators and
654 MCP detectors, and lowering the neutron energy thresh-
655 old by further minimizing the impact of the electric fields
656 on the trajectories of the recoil ions. The latter will be ac-
657 complished by bringing the electrodes closer to the center
658 of the ion trap to allow for a lower-amplitude RF voltage
659 to be applied, thus reducing the perturbation of the ion
660 trajectories while the ions are in transit to the MCP de-
661 tectors. Future experiments will also benefit from the in-
662 creased intensities and purities of the beams delivered by
663 the CARIBU facility [56, 57]; since these measurements
664 were performed, the beam intensities have increased by
665 an order of magnitude. These improvements will allow
666 βn measurements to be performed for neutron-rich nu-
667 clei even further from stability, providing access to many
668 of the isotopes that significantly impact r -process nucle-
669 osynthesis.

670 V. ACKNOWLEDGMENTS

671 We acknowledge and appreciate the assistance of the
672 ATLAS staff. This material is based upon work sup-
673 ported by the Department of Energy, National Nuclear
674 Security Administration, under Award Numbers DE-
675 NA0000979 (NSSC), DE-AC52-07NA27344 (LLNL), and
676 DE-NA0002135 (SSGF); Office of Nuclear Physics Con-
677 tract DE-AC02-06CH11357 (ANL); NEUP Project Num-
678 ber 13-5485 (University of California); Grant DE-FG02-
679 94ER40834 (University of Maryland); Louisiana State
680 Board of Regents Research Competitiveness Subprogram
681 LEQSF(2016-19)-RD-A-09; NSERC, Canada, under Ap-
682 plication No. 216974; NSF contract PHY-1419765; and
683 the Department of Homeland Security.

684 [1] E. M. Burbidge, G. R. Burbidge, W. A. Fowler, and
685 F. Hoyle, *Rev. Mod. Phys.* **29**, 547 (1957).

686 [2] A. G. W. Cameron, *Publ. Astron. Soc. Pac.* **69**, 201
687 (1957).

- [3] B. S. Meyer, G. J. Mathews, W. M. Howard, S. E. Woosley, and R. D. Hoffman, *Astrophys. J.* **399**, 656 (1992).
- [4] K. Farouqi, K.-L. Kratz, B. Pfeiffer, T. Rauscher, F.-K. Thielemann, and J. W. Truran, *Astrophys. J.* **712**, 1359 (2010).
- [5] S. Goriely, A. Bauswein, and H.-T. Janka, *The Astrophys. J.* **738**, L32 (2011).
- [6] E. Pian, P. D'Avanzo, S. Benetti, M. Branchesi, E. Brocato, S. Campana, E. Cappellaro, S. Covino, V. D'Elia, J. P. U. Fynbo, *et al.*, *Nature* **551**, 67 (2017).
- [7] S. Das, *Prog. Nucl. Energy* **28**, 209 (1994).
- [8] A. D'Angelo, *Prog. Nucl. Energy* **41**, 1 (2002).
- [9] K.-L. Kratz, *Nucl. Phys. A* **417**, 447 (1984).
- [10] S. Raman, B. Fogelberg, J. A. Harvey, R. L. Macklin, P. H. Stelson, A. Schröder, and K.-L. Kratz, *Phys. Rev. C* **28**, 602 (1983).
- [11] J. H. Hamilton, P. G. Hansen, and E. F. Zganjar, *Rep. Prog. Phys.* **48**, 631 (1985).
- [12] J. A. Winger, S. V. Ilyushkin, K. P. Rykaczewski, C. J. Gross, J. C. Batchelder, C. Goodin, R. Grzywacz, J. H. Hamilton, A. Korgul, W. Królas, *et al.*, *Phys. Rev. Lett.* **102**, 142502 (2009).
- [13] A. C. Pappas and T. Sverdrup, *Nucl. Phys. A* **188**, 48 (1972).
- [14] K.-L. Kratz, W. Rudolph, H. Ohm, H. Franz, M. Zendel, G. Herrmann, S. G. Prussin, F. M. Nuh, A. A. Shihab-Eldin, D. R. Slaughter, W. Halverson, and H. V. Klapdor, *Nucl. Phys. A* **317**, 335 (1979).
- [15] T. Kawano, P. Möller, and W. B. Wilson, *Phys. Rev. C* **78**, 054601 (2008).
- [16] E. A. McCutchan, A. A. Sonzogni, T. D. Johnson, D. Abriola, M. Birch, and B. Singh, *Phys. Rev. C* **86**, 041305 (2012).
- [17] R. M. Yee, N. D. Scielzo, P. F. Bertone, F. Buchinger, S. Caldwell, J. A. Clark, C. M. Deibel, J. Fallis, J. P. Greene, S. Gulick, *et al.*, *Phys. Rev. Lett.* **110**, 092501 (2013).
- [18] N. D. Scielzo, G. Li, M. G. Sternberg, G. Savard, P. F. Bertone, F. Buchinger, S. Caldwell, J. A. Clark, J. Crawford, C. M. Deibel, *et al.*, *Nucl. Instrum. Methods Phys. Res. A* **681**, 94 (2012).
- [19] N. D. Scielzo, R. M. Yee, P. F. Bertone, F. Buchinger, S. A. Caldwell, J. A. Clark, A. Czeszumaska, C. M. Deibel, J. P. Greene, S. Gulick, *et al.*, *Nucl. Data Sheets* **120**, 70 (2014).
- [20] G. Savard, S. Baker, C. Davids, A. F. Levand, E. F. Moore, R. C. Pardo, R. Vondrasek, B. J. Zabransky, and G. Zinkann, *Nucl. Instrum. Methods Phys. Res. B* **266**, 4086 (2008).
- [21] A. Czeszumaska *et al.*, (in preparation).
- [22] M. R. Mumpower, R. Surman, G. C. McLaughlin, and A. Aprahamian, *Prog. Part. Nucl. Phys.* **86**, 86 (2016).
- [23] C. N. Davids and D. Peterson, *Nucl. Instrum. Methods Phys. Res. B* **266**, 4449 (2008).
- [24] G. Savard, R. C. Barber, D. Beeching, F. Buchinger, J. E. Crawford, S. Gulick, X. Feng, E. Hagberg, J. C. Hardy, V. T. Koslowsky, *et al.*, *Nucl. Phys. A* **626**, 353 (1997).
- [25] J. C. Wang, G. Savard, K. S. Sharma, J. A. Clark, Z. Zhou, A. F. Levand, C. Boudreau, F. Buchinger, J. E. Crawford, J. P. Greene, *et al.*, *Nucl. Phys. A* **746**, 651 (2004).
- [26] B. Singh, A. A. Rodionov, and Y. L. Khazov, *Nucl. Data Sheets* **109**, 517 (2008).
- [27] A. A. Sonzogni, *Nucl. Data Sheets* **95**, 837 (2002).
- [28] N. Nica, *Nucl. Data Sheets* **108**, 1287 (2007).
- [29] W. Paul, *Rev. Mod. Phys.* **62**, 531 (1990).
- [30] J. L. Wiza, *Nucl. Instrum. Methods* **162**, 587 (1979).
- [31] M. Lampton and C. W. Carlson, *Rev. Sci. Instrum.* **50**, 1093 (1979).
- [32] K. Siegl, N. D. Scielzo, A. Czeszumaska, J. A. Clark, G. Savard, A. Aprahamian, S. A. Caldwell, B. S. Alan, M. T. Burkey, C. J. Chiara, *et al.*, *Phys. Rev. C* **97**, 035504 (2018).
- [33] A. Czeszumaska, Ph.D. thesis, University of California, Berkeley, Department of Nuclear Engineering (2016).
- [34] N. D. Scielzo, S. J. Freedman, B. K. Fujikawa, and P. A. Vetter, *Phys. Rev. A* **68**, 022716 (2003).
- [35] J. M. Munson, K. Siegl, N. D. Scielzo, B. S. Alan, A. Czeszumaska, G. Savard, A. Aprahamian, S. A. Caldwell, C. J. Chiara, J. A. Clark, *et al.*, *Nucl. Instrum. Methods Phys. Res. A* **898**, 60 (2018).
- [36] B. Holstein, *Rev. Mod. Phys.* **46** (1974).
- [37] P. Hoff, B. Ekström, and B. Fogelberg, *Z. Phys. A* **332**, 407 (1989).
- [38] S. Agostinelli, J. Allison, K. Amako, J. Apostolakis, H. Araujo, P. Arce, M. Asai, D. Axen, S. Banerjee, G. Barrand, *et al.*, *Nucl. Instrum. Methods Phys. Res. A* **506**, 250 (2003).
- [39] J. Allison, K. Amako, J. Apostolakis, H. Araujo, P. Arce Dubois, M. Asai, G. Barrand, R. Capra, S. Chauvie, R. Chytraccek, *et al.*, *IEEE Trans. Nucl. Sci.* **53**, 270 (2006).
- [40] D. Manura and D. Dahl, *SIMION 8.0/8.1 User Manual (Scientific Instrument Services, Inc. Ringoes, NJ 08551)* (2008).
- [41] S. Shalev and G. Rudstam, *Nucl. Phys. A* **230**, 153 (1974).
- [42] S. Shalev and G. Rudstam, *Nucl. Phys. A* **275**, 76 (1977).
- [43] S. A. Caldwell, Ph.D. thesis, University of Chicago, Department of Physics (2015).
- [44] L. Tomlinson and M. H. Hurdus, *J. Inorg. Nucl. Chem.* **30**, 1649 (1968).
- [45] W. Rudolph, K.-L. Kratz, and G. Herrmann, *J. Inorg. Nucl. Chem.* **39**, 753 (1977).
- [46] J. Crançon, C. Ristori, H. Ohm, W. Rudolph, K.-L. Kratz, and M. Asghar, *Z. Phys. A* **287**, 45 (1978).
- [47] H.-D. Schüssler and G. Herrmann, *Radiochim. Acta* **18**, 123 (1972).
- [48] K.-L. Kratz and G. Herrmann, *Nucl. Phys. A* **229**, 179 (1974).
- [49] K.-L. Kratz, *Radiochim. Acta* **25**, 1 (1978).
- [50] E. Lund, P. Hoff, K. Aleklett, O. Glomset, and G. Rudstam, *Z. Phys. A* **294**, 233 (1980).
- [51] G. Rudstam, K. Aleklett, and L. Sihver, *At. Data Nucl. Data Tables* **53**, 1 (1993).
- [52] B. Pfeiffer, K.-L. Kratz, and P. Möller, *Prog. Nucl. Energy* **41**, 39 (2002).
- [53] R. Caballero-Folch, I. Dillmann, J. Agramunt, J. L. Taín, A. Algora, J. Äystö, F. Calviño, L. Canete, G. Cortés, C. Domingo-Pardo, *et al.*, *Phys. Rev. C* **98**, 034310 (2018).
- [54] K. Aleklett, P. Hoff, E. Lund, and G. Rudstam, *Z. Phys. A* **295**, 331 (1980).
- [55] R. Surman, M. Mumpower, and A. Aprahamian, *JPS Conf. Proc.* **6**, 010010 (2015), <https://journals.jps.jp/doi/pdf/10.7566/JPSCP.6.010010>.

- ⁸¹⁵ [56] T. Y. Hirsh, N. Paul, M. Burkey, A. Aprahamian, ⁸¹⁹ [57] G. Savard, A. F. Levand, and B. J. Zabransky, Nucl.
⁸¹⁶ F. Buchinger, S. Caldwell, J. A. Clark, A. F. Levand, ⁸²⁰ Instrum. Methods Phys. Res. B **376**, 246 (2016).
⁸¹⁷ L. L. Ying, S. T. Marley, *et al.*, Nucl. Instrum. Methods
⁸¹⁸ Phys. Res. B **376**, 229 (2016).